k Dependence of the Crystal-Field Splittings of $4f$ States in Rare-Earth Systems

D. V. Vyalikh,[1] S. Danzenbächer,[1] Yu. Kucherenko,[1,2] K. Kummer,[1] C. Krellner,[3] C. Geibel,[3] M. G. Holder,[1] T. K. Kim,[4] C. Laubschat,[1] M. Shi,[5] L. Patthey,[5] R. Follath,[6] and S. L. Molodtsov[1,7]

[1]*Institut für Festkörperphysik, Technische Universität Dresden, D-01062 Dresden, Germany*
[2]*Institute for Metal Physics, National Academy of Sciences of Ukraine, UA-03142 Kiev, Ukraine*
[3]*Max-Planck-Institut für Chemische Physik fester Stoffe, Nöthnitzer Strasse 40, D-01187 Dresden, Germany*
[4]*Leibniz-Institute for Solid State Research, IFW-Dresden, D-01171 Dresden, Germany*
[5]*Swiss Light Source, Paul Scherrer Institute, CH-5232 Villigen-PSI, Switzerland*
[6]*Helmholtz-Zentrum Berlin für Materialien und Energie GmbH, Elektronenspeicherring BESSY II, D-12489 Berlin, Germany*
[7]*European XFEL GmbH, Albert-Einstein-Ring 19, D-22671 Hamburg, Germany*

(Received 27 June 2010; revised manuscript received 19 October 2010; published 3 December 2010)

The occupation, energy separation, and order of the crystal-field-split $4f$ states are crucial for the understanding of the magnetic properties of rare-earth systems. We provide the experimental evidence that crystal-field-split $4f$ states exhibit energy dispersion in momentum space leading to variations of energy spacings between them and even of their energy sequence across the Brillouin zone. These observations were made by performing angle-resolved photoemission experiments on $YbRh_2Si_2$ and properly simulated within a simple model based on results obtained by inelastic neutron scattering experiments and band structure calculations. Our findings should be generally applicable to rare-earth systems and have considerable impact on the understanding of magnetism and related phenomena.

DOI: 10.1103/PhysRevLett.105.237601 PACS numbers: 79.60.−i, 71.27.+a, 71.70.Ch

The magnetic properties of rare-earth (RE) materials strongly depend on the partly filled $4f$ shells which lie deep inside the ionic cores, do not overlap with each other, and, therefore, maintain most of their atomic properties in the solid. In the free atom a $4f$ ground state with a well-defined occupancy n and total angular momentum J is found, separated from other configurations by Coulomb repulsion and spin-orbit interaction energies of the order of several eV [1]. In a solid, however, this atomic ground state is further narrowly split due to the interaction with the nonspherical electrostatic field of the ligands, which is called the crystal electric field (CEF) [2,3]. As a consequence, the wave functions of the ground and the excited states of the $4f$ shell as well as the corresponding excitation energies sensitively depend on the structure and composition of the specific compound. Since the CEF splittings are only of the order of 10 meV, excited states may be thermally populated which leads to many outstanding properties of RE materials.

Apart from the $4f$ occupancy, the number, energy separation, energy order, and degeneracy of the CEF levels are of highest importance for the understanding of the magnetic properties of RE materials. Respective information is usually obtained from inelastic neutron scattering experiments [4,5] and analyzed in the light of CEF-related approaches, which consider the electrostatic interactions of purely atomic $4f$ orbitals with the charge distribution of the solid [2,3]. But despite their localized nature, $4f$ states are able to hybridize with valence states in a solid via hopping interactions, which can cause pronounced deviations from their atomic properties [6,7], leading to a variety of exotic many-body phenomena [8–10]. Since the valence states in a crystalline solid form dispersing bands (VBs) that continuously change both their energy E and their symmetry properties as a function of the wave vector $\boldsymbol{k}$, the interaction with the $4f$ states may become $\boldsymbol{k}$-dependent, too [6,7]. This may induce a dispersion of the CEF-split $4f$ states, causing variations of the energy spacings and even changes in the sequence of the CEF levels across the Brillouin zone (BZ). Respective effects are hardly observable by means of inelastic neutron scattering or resonant methods that integrate over electron excitations in $\boldsymbol{k}$ space but may have severe impact on the understanding of all kinds of low-energy excitations and, in particular, of the magnetic properties of RE systems.

Angle-resolved photoemission (ARPES) can usually not provide information on near-ground state properties of a $4f$ system because the excited $4f^{n-1}$ final states are energy shifted with respect to the $4f^n$ initial states by several eV and, therefore, undergo completely different interactions with the VBs. In mixed-valent or heavy-fermion systems, however, where the $4f^n$ and $4f^{n-1}$ electron configurations are mixed in the ground state, the initial state configuration is reproduced by some of the $4f^{n-1}$ final states making near-ground state properties like $\boldsymbol{k}$ dependence of CEF splittings accessible to the experiment.

In the present Letter, we report the direct observation of the CEF splitting of the magnetically relevant $4f^{13}$ state in the heavy-fermion compound $YbRh_2Si_2$ [11–13]. In addition to a general dispersion of the $4f$ states including a Fermi-energy (E_F) crossing at the $\bar{\Gamma}$ point reported in our previous publications [7,14], a clear $\boldsymbol{k}$ dependence of the

individual CEF-split states is observed that leads to variations of the energy splittings across the BZ and even to interchange of the $\Gamma_{t6}^{(1)}$ and $\Gamma_{t7}^{(1)}$ ground states around the $\bar{\Gamma}$ point. The experimental data are well reproduced in the framework of a simple hybridization model using atomic CEF splittings as extracted from inelastic neutron scattering in light of the ligand-field theory and the $\boldsymbol{k}$ dependence of the VB structure as obtained from linear-muffin-tin-orbital calculations as the input parameters. As has been shown in previous studies, the hybridization parameter used in the model to describe the interaction of the $4f$ and VB states varies only slightly across the RE series [15]. Thus, conclusions derived from this Yb-based compound are expected to also be valid for other, particularly stable-valent RE systems, where near-ground state properties are not accessible for photoemission (PE).

The measurements were performed at BESSY by using the "1^3-ARPES" instrument and at the Swiss Light Source (Surface and Interface Spectroscopy beam line). The geometry of the experiment includes a fixed analyzer and a rotatable, vertically mounted sample [6,7,14]. The polar-angle rotation axis together with the direction of the analyzer slit was perpendicular to the plane of the storage rings. To disclose symmetry of the CEF-split $4f$ states, we applied (i) the phenomenon of the "geometric" dichroism in angle-resolved photoemission using circularly polarized light with both helicities [14] and (ii) parity selection rules for the excitation using linearly polarized light with the electric vector aligned horizontally and vertically with respect to the storage-ring plane of the facilities.

An ARPES-derived band map of Si-terminated $YbRh_2Si_2$ [7], recorded along the $\bar{\Gamma}$-$\bar{X}$ direction of the surface BZ at temperatures $\sim$1 K (BESSY's instrument), using a photon energy of $h\nu = 45$ eV and linear vertical light polarization with respect to the storage-ring plane, is shown in Fig. 1(a). It reveals a bunch of four weakly dispersive states closely below the E_F interacting with at least two holelike, parabolic bands, labeled **1** and **2**, around the $\bar{\Gamma}$ point. The parabolic bands are mainly derived from Rh $4d$ states and overlap each other at the $\bar{\Gamma}$ point where they show a particularly large intensity. The weakly dispersing states labeled I–IV are derived from the $^2F_{7/2}$ multiplet term of the Yb $4f^{13}$ final state configuration that is degenerate in energy with the $4f^{14}$ configuration in the ground state and, therefore, appears close to zero binding energy (BE) in the ARPES experiment. The tetragonal crystal field acting on the Yb atoms in $YbRh_2Si_2$ splits this $^2F_{7/2}$ term into four Kramers doublets related to the irreducible representations $\Gamma_{t6}^{(1)}$, $\Gamma_{t6}^{(2)}$, $\Gamma_{t7}^{(1)}$, and $\Gamma_{t7}^{(2)}$. The wave functions of the respective states are linear combinations of spherical spinors with $m_j = \pm 1/2, \pm 7/2$ for Γ_{t6} and $m_j = \pm 3/2, \pm 5/2$ for Γ_{t7}. The energy splittings between these states are known from neutron scattering experiments [16] and amount to 17, 25, and 43 meV relative to the ground state, which is in accordance with the observed separations of states II–IV with respect to state I away from the $\bar{\Gamma}$ point. It remained unclear whether $\Gamma_{t6}^{(1)}$, where $m_j = \pm 1/2$ states dominate, or $\Gamma_{t7}^{(1)}$ with domination of $m_j = \pm 3/2$ states forms the ground state I [17,18]. In any case, the highest excited state IV can be assigned to $\Gamma_{t6}^{(2)}$ (strongly dominated by $m_j = \pm 7/2$ states). The fourth component, $\Gamma_{t7}^{(2)}$, containing mostly $m_j = \pm 5/2$ states, may then be assigned either to state II or III.

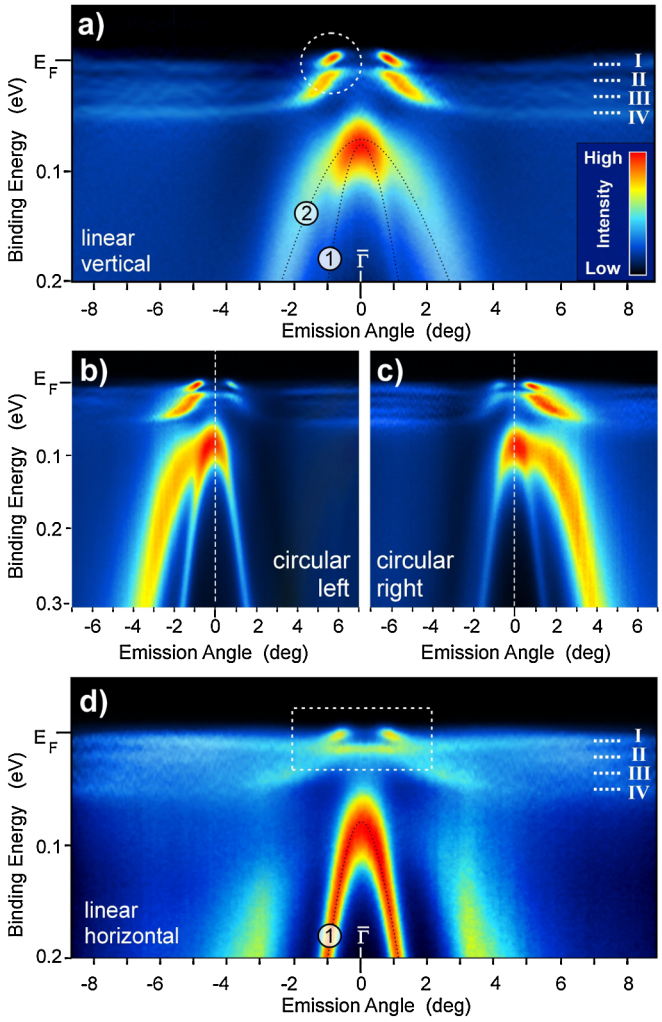

FIG. 1 (color online). ARPES spectra taken from the Si-terminated surface of $YbRh_2Si_2$ along the $\bar{\Gamma}$-$\bar{X}$ direction of the surface BZ using 45 eV photons and linear vertical (a), circular left (b), circular right (c), and linear horizontal (d) polarization.

Our ARPES data show that the picture of four non-dispersive Kramers doublets with well-defined energy order becomes drastically disturbed when the $\bar{\Gamma}$ point of the BZ is approached. There the bunch of CEF-split $4f$ states seems to be pushed towards lower BE due to the interaction with the parabolic bands. Moreover, even a crossing of E_F is detected, indicating lacking $4f^{14}$ admixture to the ground state in this region of the $\boldsymbol{k}$ space. The induced dispersion of the $4f$ states is accompanied by an

enhancement of their PE intensities, pointing to an increase of photoionization cross section caused by Rh $4d$ admixtures to their wave functions. The shape of the outer parabolic band **2** appears to be flattened, giving the impression that without interaction with the $4f$ states this band would extend towards lower BE or even cross E_F. The shape of the inner band **1**, on the other hand, does not seem to be notably deformed.

Such avoided crossing behavior is typical for the interaction of electronic states characterized by the same symmetry of their wave functions. In ARPES experiments, states with the same symmetry can be identified by their similar response to a change of light polarization. Matrix elements for excitation of a photoelectron from, e.g., even-symmetry states with circularly left or circularly right polarized light are affected by possible admixture of odd-symmetry wave functions and vice versa. This will cause dichroic effects differing in sign for positive and negative $\boldsymbol{k}$, and states with the same dichroic response to a change of circular polarization can be assumed to have similar symmetry properties [14,19,20].

This can be seen in Figs. 1(b) and 1(c) where ARPES data taken with left and right circular polarization, respectively, are depicted. Apparently, the parabolic band **2** is subject to dichroism, whereas band **1** is not essentially affected by the change of light polarization. Moreover, close to the $\bar{\Gamma}$ point the two most intense CEF-split $4f$ states show dichroism similar to band **2**. This points to similar symmetries of the three which would explain why they avoid crossing each other and form hybridization gaps instead. On the other hand, there are other CEF-split $4f$ states that do not follow the dichroic behavior of the discussed two CEF-split states and, therefore, shall have a different symmetry and be allowed to cross them. By looking at the ARPES map in Fig. 1(d) taken with linear horizontal polarization, this is evidently the case.

More information on the symmetry properties of the parabolic bands can be gained from respective slab calculations simulating the layered structure of $YbRh_2Si_2$ [7]. Figure 2(a) shows the calculated $4d$ bands derived from subsurface Rh atoms within the first 20% of the $[\bar{\Gamma}\text{-}\bar{X}]$ distance. Similar to Fig. 1, two holelike bands (black and gray dots) are seen close to E_F at the $\bar{\Gamma}$ point. While the gray-dotted band is in full agreement with the experimental band **1**, the black-dotted band **2** lies at lower BE than in the ARPES measurements and its top is found above E_F, as would be anticipated from the ARPES data if interactions with the $4f$ states were absent. Additionally, an unoccupied electronlike band **3** emerges from our calculations that may affect the dispersion of the $4f$ states.

Hybridization with the localized Yb $4f$ states can predominantly occur from the Rh $4d_{xz,yz}$ orbitals that are oriented towards the atoms of the adjacent Yb layer and contribute to bands **2** and **3**, whereas band **1** mainly derived from in-plane $4d_{xy}$ states is not expected to interact with the $4f$ states. Given that the shape of band **2** is flattened and its top is shifted to higher BE due to f-d interaction, while neither was observed for band **1**, this is in good agreement with the experimental observations. In order to identify the CEF-split $4f$ states mainly affected by f-d hybridization, we analyzed the local symmetry of the Rh $4d$ states at the Yb sites. Our calculations show that here f states with quantum numbers $m = \pm 3$ in the case of band **2** and $m = \pm 1$ in the case of band **3** dominate, so that $\Gamma_{t6}^{(2)}$ (more than 80% $m = \pm 3$ orbital contributions) and $\Gamma_{t7}^{(1)}$ (more than 60% $m = \pm 1$ orbital contributions) may be affected, respectively.

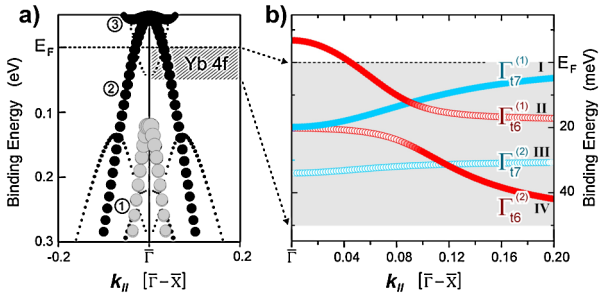

FIG. 2 (color online). (a) Valence bands deriving from subsurface Rh atoms calculated for a Si-terminated slab of $YbRh_2Si_2$ along the $\bar{\Gamma}$-$\bar{X}$ direction of the surface BZ. Yb $4fs$ were treated as quasicore states. The dot size scales with the Rh $4d$ contributions. (b) Dispersion of the crystal-field-split Yb $4f$ states simulated within the hybridization model.

From Fig. 1(d), it can be seen that the CEF ground state I is clearly pushed slightly downwards in energy at the $\bar{\Gamma}$ point, suggesting its interaction with the unoccupied electronlike band **3** [Fig. 2(a)]. We can thus assign it to $\Gamma_{t7}^{(1)}$. Similarly, the expected avoided crossing and formation of a hybridization gap between state IV (already identified as $\Gamma_{t6}^{(2)}$) and band **2** is evident from the experimental data [Fig. 1(a)].

In contrast, hybridization with Rh $4d$ bands cannot explain the appearance of an energy gap between two CEF states clearly seen in Fig. 1(a). However, taking into account that four CEF states belong to two irreducible representations (Γ_{t6} and Γ_{t7}), we could also expect the avoided crossing behavior between two Kramers doublets of the same symmetry.

In order to disentangle the observed phenomena, we simulated the Rh $4d$ bands and Yb $4f$ states around the $\bar{\Gamma}$ point in the framework of the following model: The Rh $4d$ bands **1**–**3** were approximated by parabolas fitted to the results of our slab calculations [Fig. 2(a)]. The energy of the CEF-split $4f$ states was taken from inelastic neutron scattering experiments [16]. Then we introduced interaction between the VBs and $4fs$ with the same symmetry, i.e., between band **2** and state IV ($\Gamma_{t6}^{(2)}$) as well as between band **3** and state I ($\Gamma_{t7}^{(1)}$), characterized by a parameter $\Delta_{fd} = 40$ meV that was estimated from the experimental hybridization gap between band **2** and state IV (see Fig. 1).

As a result, gaps formed and the CEF-split states I and IV were forced into a rather weak electron- and strong hole-like dispersion, respectively. In order to account for interaction between the CEF-split $4f$ states, we also introduced a hybridization Δ_{ff} between pairs belonging to the same irreducible representation (to Γ_{t6} or to Γ_{t6}). The best agreement with the experimentally observed data was achieved by setting Δ_{ff} to 8 meV.

The obtained results are shown in Fig. 2(b). Evidently, the applied model convincingly describes all features of the ARPES spectra. For instance, the CEF-split $4f$ state IV undergoes strong hybridization with the valence band **2** and is pushed upwards at the $\bar{\Gamma}$ point. A degeneration of the IV and II states is prohibited due to the same symmetry (Γ_{t6}) which leads to avoided crossing and formation of a gap between the two respective dispersion lines observed in ARPES (cf. Fig. 1). Also, since states I, II, and IV were assigned to three of the four Kramers doublets, we can now assign state III to the only remaining possibility, i.e., $\Gamma_{t7}^{(2)}$.

One could try to emphasize or weaken the dispersive behavior imposed on the CEF-split $4f$ states by changing the position of the parabolic bands. This can, for instance, be done by substituting Rh in $YbRh_2Si_2$ by the formally isoelectronic elements Co or Ir [21]. Here we achieved respective band shifts by remeasuring the ARPES data not exactly along the $\bar{\Gamma}$-$\bar{X}$ direction of the BZ but along slightly shifted directions parallel to $\bar{\Gamma}$-$\bar{X}$. The obtained spectra with shifted VBs are shown in the upper panels of Fig. 3. Apparently, already small shifts of band **2** towards higher BE severely attenuate their hybridization with the CEF-split Yb $4f$ states. As a result, the dispersion of the latter is flattened and E_F is no longer crossed. If the bands are shifted even further away from E_F, no hybridization gap between states II and IV will be visible either (not shown). The respective simulations with adopted band positions, but the same hybridization parameters $\Delta_{fd} = 40$ meV and $\Delta_{ff} = 8$ meV, perfectly reproduce these experimental observations (lower panels in Fig. 3). Beyond that, we were also able to simulate the $\boldsymbol{k}$-dependent intensity variations of the CEF $4f$ states, accounting for the fact that increasing Rh $4d$ admixture to $4f$ states will cause a proportional enhancement of their PE intensity by virtue of the much higher photoionization cross section of Rh $4d$ states [22].

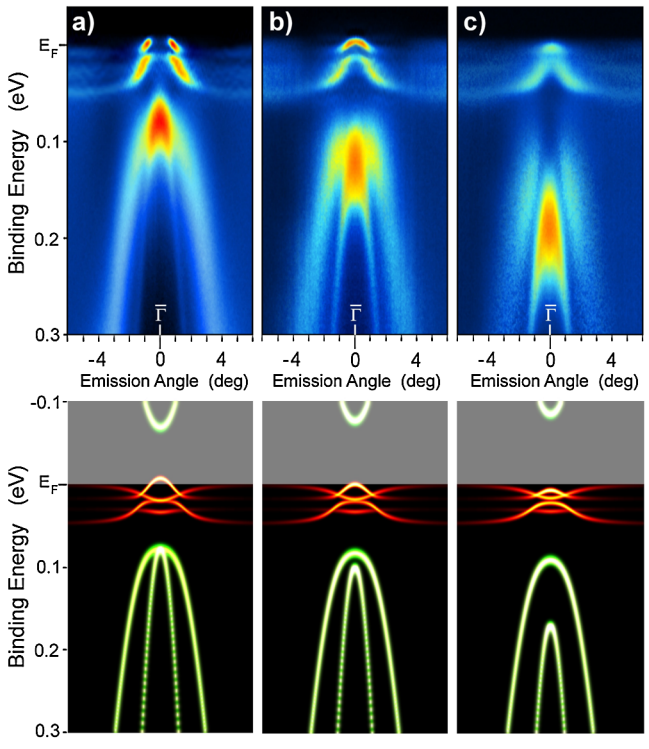

FIG. 3 (color online). Experimental (upper panels) and simulated (lower panels) ARPES spectra from the Si-terminated surface of $YbRh_2Si_2$ taken along the $\bar{\Gamma}$-$\bar{X}$ direction (a) and along parallel directions shifted from the $\bar{\Gamma}$ point by about 0.03 (b) and 0.06 (c) of the [$\bar{\Gamma}$-$\bar{X}$] distance.

This work was supported by the DFG (Grants No. VY 64/1-1 and No. GE 602/2-1) as well as by the Science and Technology Center in Ukraine (Grant No. 4930). The authors thank A. Varykhalov and AG Borisenko for their support at the "1^3-ARPES" beam line of BESSY II.

[1] J. Jensen and A. R. Mackintosh, *Rare Earth Magnetism—Structures and Excitations* (Clarendon, Oxford, 1991).
[2] P. Fulde and M. Loewenhaupt, Adv. Phys. **34**, 589 (1985).
[3] U. Walter, Z. Phys. B **62**, 299 (1986).
[4] A. Severing *et al.*, Phys. Rev. B **41**, 1739 (1990).
[5] E. A. Goremychkin and R. Osborn, Phys. Rev. B **47**, 14 280 (1993).
[6] S. Danzenbächer *et al.*, Phys. Rev. Lett. **102**, 026403 (2009).
[7] D. V. Vyalikh *et al.*, Phys. Rev. Lett. **103**, 137601 (2009).
[8] J. M. Lawrence, P. S.Riseborough, and R. D. Parks, Rep. Prog. Phys. **44**, 1 (1981).
[9] N. Andrei, K. Furuya, and J. H. Lowenstein, Rev. Mod. Phys. **55**, 331 (1983).
[10] G. R. Stewart, Rev. Mod. Phys. **56**, 755 (1984).
[11] P. Coleman and A. J. Schofield, Nature (London) **433**, 226 (2005).
[12] P. Gegenwart, Q. Si, and F. Steglich, Nature Phys. **4**, 186 (2008).
[13] O. Trovarelli *et al.*, Phys. Rev. Lett. **85**, 626 (2000).
[14] D. V. Vyalikh *et al.*, Phys. Rev. Lett. **100**, 056402 (2008).
[15] S. L. Molodtsov *et al.*, Phys. Rev. B **68**, 193101 (2003); Yu. Kucherenko *et al.*, Phys. Rev. B **70**, 045105 (2004).
[16] O. Stockert *et al.*, Physica (Amsterdam) **378B–380B**, 157 (2006).
[17] A. S. Kutuzov *et al.*, J. Phys. Condens. Matter **20**, 455208 (2008).
[18] A. M. Leushin and V. A. Ivanshin, Physica (Amsterdam) **403B**, 1265 (2008).
[19] C. M. Varma, Phys. Rev. B **73**, 233102 (2006).
[20] S. V. Borisenko *et al.*, Phys. Rev. Lett. **92**, 207001 (2004).
[21] S. Danzenbächer *et al.*, Phys. Rev. B **75**, 045109 (2007).
[22] J. J. Yeh and I. Lindau, At. Data Nucl. Data Tables **32**, 1 (1985).